Published in final edited form as:
J Comp Neurol. 2004 December 13; 480(3): 251–263. doi:10.1002/cne.20330.

DARPP-32-like immunoreactivity in AII amacrine cells of rat retina

Gloria J. Partida, **Sherwin C. Lee**, **Leah Haft-Candell**, **Grant S. Nichols**, and **Andrew T. Ishida***
Section of Neurobiology, Physiology, and Behavior, University of California, Davis, CA 95616-8519

Abstract

Previous studies demonstrated that the dopamine- and adenosine 3′,5′-monophosphate-regulated phosphatase inhibitor known as “DARPP-32” is present in rat, cat, monkey, and human retinas. We have followed up these studies by asking what specific cell subtypes contain DARPP-32. Using a polyclonal antibody directed against a peptide sequence of human DARPP-32, we immunostained adult rat retinas that were either transretinally sectioned or flat-mounted, and found DARPP-32-like immunoreactivity in some cells of the amacrine cell layer across the entire retinal surface. Based on the shape and spatial distribution of these cells, their staining by an anti-parvalbumin antibody, and their juxtaposition with processes containing tyrosine hydroxylase, we report here that DARPP-32-like immunoreactivity is present in AII amacrine cells of rat retina. These results suggest that the response of AII amacrine cells to dopamine is not mediated as simply as previously supposed.

Keywords

dopamine; glycine; phosphatase inhibitor; inner retina; light adaptation

INTRODUCTION

A multifaceted series of studies over the past 20 years has shown that dopamine can modulate the phosphorylation of neuronal proteins by regulating protein kinase and protein phosphatase activities (Greengard et al., 1999). Two of these types of dopamine response have been found to involve a 32-kD phosphoprotein known as "DARPP-32". In one, D1-type dopamine receptor activation leads to an increase in cAMP production, and DARPP-32 is transformed into a potent inhibitor of protein phosphatase 1 ("PP-1") when phosphorylated by cAMP-dependent protein kinase (“PKA”). This allows dopamine to regulate ion channels, neurotransmitter receptors, ion pumps, and transcription factors by a combination of direct phosphorylation of these effector proteins (by PKA) and inhibition (by phospho-DARPP-32) of their dephosphorylation (e.g., Surmeier et al., 1994; Schiffmann et al., 1995, 1998; Yan et al., 1999; Nishi et al., 2000). In a second type of dopamine response, D2-type receptor activation regulates protein function by decreasing cAMP production and by activating the calcium/calmodulin-dependent protein phosphatase "calcineurin" which dephosphorylates and inactivates DARPP-32 (Nishi et al., 1997, 2002).

The properties, distribution and functional importance of DARPP-32 are known almost entirely from studies of several brain regions and from consequences in knock-out mice

*Correspondence to: Andrew Ishida at the address given above, tel & fax: (530) 752-3569, atishida@ucdavis.edu.

(Walaas and Greengard 1984; Hemmings et al., 1984a,b; Hemmings and Greengard 1986; Fienberg et al., 1998). Much less is known about the disposition of DARPP-32 in the retina, even though (*i*) the concentration of DARPP-32 in the retina is comparable to levels in frontal cortex and hippocampus (Hemmings and Greengard 1986), (*ii*) dopaminergic interneurons (either amacrine or interplexiform cells) are thought to innervate the retinas of all vertebrate classes (Ehinger 1983; Brecha 1983; Marc 1995), and (*iii*) a wide variety of effects of dopamine on retinal synaptic pathways and signal processing have been known for several years (Dowling 1991; Witkovsky and Dearry 1991). One previous study immunostained cat, monkey, and human retinas for DARPP-32, and found DARPP-32-like immunoreactivity in some cell bodies in the inner nuclear layer, adjacent to the inner plexiform layer (IPL), as well as in some somata in the optic fiber layer (Meister et al., 1991). Because no somata in the ganglion cell layer were stained, the DARPP-32 immunopositive cells adjacent to the IPL appeared to be amacrine cells rather than displaced ganglion cells. Because stained cells were separated by unstained cells (particularly in cat and monkey retinas), the staining pattern suggested that DARPP-32 might be present in only some amacrine cells.

In the present study, we have asked what cell subtypes contain DARPP-32, and found four lines of evidence that, in adult rat retina, DARPP-32 is present in AII amacrine cells. These results are of interest because AII amacrine cells are one of several retinal cell types known to be dopamine-sensitive (Dowling 1991; Witkovsky and Dearry 1991; Hampson et al., 1992; Mills and Massey 1995), and because dopamine alters the ability of AII amacrine cells to relay rod bipolar cell signals to cone bipolar cells (and, thus, their ability to help route rod photoreceptor signals to ganglion cells; see Bloomfield and Dacheux 2001).

METHODS

Animals

Adult rat retinas were used for all of the experiments reported here for a number of reasons: the presence, synthesis, and release of dopamine, as well as dopamine receptor activation and regulation of cAMP, have been demonstrated; the anatomy and distribution of dopamine-sensitive cell types are known; and depletion of dopamine has a conspicuous behavioral effect (Malmfors, 1963; Häggendahl and Malmfors 1965; Pycock and Smith 1983; Voigt and Wässle 1987; Wässle et al., 1993; Bjelke et al. 1996; Shulman and Fox 1996; Feigenspan et al., 2001; Puopolo et al., 2001; Patel et al., 2003). Sprague-Dawley rats (female; P60-P120; 150–250 g) were obtained from a commercial supplier (Harlan Bioproducts; Indianapolis, IN) and housed in standard cages at room temperature (~23 °C) on a 12-hr/12-hr light/dark cycle. Prior to enucleation of each eye, rats were sacrificed by a lethal dose of sodium pentobarbital (50 mg/ml; 1.5 cc/kg, i.p.). All animal care and experimental protocols were approved by the Animal Use and Care Administrative Advisory Committee of the University of California, Davis.

Protein isolation

Retinas were placed individually in thin-walled eppendorf tubes immediately following separation from the vitreous and eyecup, and frozen by dropping into liquid nitrogen. Fifteen to forty retinas were then put into a tissue grinder and collectively homogenized in ice cold lysis buffer containing 1% (w/v) sodium dodecylsulfate (SDS), 50 mM Tris (pH 8.3), 5 mM ethylenediamine tetraacetic acid (EDTA); and supplemented with a protease and phosphatase inhibitor cocktail that included 50 mM NaF, 50 mM beta glycerol phosphate (pH 8.0), 0.2 mM sodium orthovanadate, 0.1 mM L-1-Chloro-3-(4-tosylamido)-4-phenyl-2-butanone (TPCK), 10 μg/ml leupeptin and pepstatin A, 1 μg/ml aprotinin, 0.1 mg/ml benzamidine and 8 μg/ml calpain I and II inhibitors. (The sources of these and other

chemicals and antibodies used in this study are listed below.) The homogenate was allowed to sit for ten minutes on ice and then centrifuged at 13000 × g for 15 min at 4°C. The supernatant was collected and assayed, using the Bradford method, for total protein. Prior to running on a 4–20% tris glycine polyacrylamide gradient gel (Invitrogen; Carlsbad, CA), the protein extract was diluted 2:1 in Laemmli buffer [62.5 mM Tris HCl (pH 6.8), 25% (v/v) glycerol, 2% (w/v) SDS, 0.01% (v/v) bromophenol blue, 300 mM dithiothreitol (DTT)] and boiled for 5 min. The gel lanes were loaded with 50–100 μg of protein. Magic Mark and Blue Ranger protein standards were run in lanes adjacent to the protein samples.

Western Blot

After electrophoretic separation, proteins were transferred from the polyacrylamide gradient gel to a nitrocellulose membrane (0.2 μm pore diameter). The membrane was stained with Ponceau S to confirm transfer, and blocked in TBST [0.1% (v/v) Tween-20 in Tris buffered saline] containing 3% dry non-fat milk (w/v) for 1 hr at room temperature. The membrane was then divided and incubated overnight at 4°C with either anti-DARPP-32 antibody or anti-DARPP-32 antibody that had been pre-adsorbed overnight at 4°C with a two-fold higher concentration of DARPP-32 blocking peptide. After several rinses in TBST, rabbit secondary antibody conjugated to horseradish peroxidase (Amersham; Piscataway, NJ) was applied for 1 hr at room temperature and again rinsed in TBST. Protein bands were visualized using ECL detection with SuperSignal West Pico Chemiluminescent Substrate. Primary antibody and peptide-blocked antibody were diluted to a concentration of 1:1000, in TBST containing 3% BSA (w/v). Secondary antibody was diluted to a concentration of 1:1000, in TBST containing 3% milk (w/v).

Immunocytochemistry

Retinas were prepared as either transretinal (“vertical”) sections or whole (“flat”) mounts, and immunostained with antibodies against DARPP-32, parvalbumin, and/or tyrosine hydroxylase (details listed below). For studies utilizing vertical sections, eyes were slit along the ora serrata using a scalpel and immediately immersed in freshly prepared aldehyde fixative [4% w/v paraformaldehyde in phosphate-buffered saline (PBS); referred to hereafter as “4% paraformaldehyde”]. After 1 hr at room temperature, these eyes were rinsed in PBS, and kept in PBS supplemented with 30% sucrose overnight at 4°C. The eyes were then hemisected, and the lens and vitreous removed. The retina, in the eyecup, was placed in a plastic mold containing O.C.T compound, and immersed in hexane which had been cooled to just above freezing in a liquid nitrogen bath. Vertical sections were cut at a thickness of 10–12 μm on a cryostat (#CM3050; Leica; Lafayette, CA), collected onto Superfrost/Plus slides (Fisher Scientific) and stored at 4 °C until use.

Sections were rinsed three times (5 min per rinse) with PBS (pH 7.4) and covered with blocking solution consisting of 5% (v/v) normal goat serum (NGS) and 0.5% (v/v) Triton X-100 in PBS for 1 hr at room temperature. The sections were then covered with solutions containing primary antibodies, and incubated overnight at 4°C. After several washes in PBS the sections were incubated with secondary antibodies for 1 hr at room temperature. After several more washes in PBS, the sections were mounted in FluorSave reagent, overlaid with a coverslip and imaged (see below). Control experiments for staining by the anti-DARPP-32 antibody were run by processing two sets of sections from the same retina simultaneously and, except for the primary antibody, identically. One set of sections was incubated in anti-DARPP-32 antibody, while the other sections were incubated in anti-DARPP-32 antibody that had been mixed with the blocking peptide, as described above (cf., Meister et al., 1991).

For studies of whole-mount preparations, each freshly dissected eyecup was placed in 5 ml of 4% paraformaldehyde and exposed to microwave irradiation for 20 seconds in a clinical

microwave set at 750W (Pelco #34700 BioWave; Ted Pella; Redding, CA; see Gustincich et al., 1999). Thereafter, these eyecups were transferred to ice-cold 4% paraformaldehyde for 30–60 min. Each retina was then gently peeled from the eyecup, rinsed for a total of 2 hrs in PBS (replacing the PBS every 12 min) on a rocker and stored in blocking solution (5% NGS, 0.5% Triton X-100 in PBS) overnight at 4°C. These retinas were incubated in primary antibodies for 48 hours at 4°C, rinsed, as described above, and incubated in secondary antibodies for 24 hours at 4°C. After a final rinse, the retinas were laid ganglion-cell-side up on Superfrost/Plus slides, covered with FluorSave reagent and a #1 glass coverslip. To help the retinas flatten as much as possible, radial incisions were made manually, with a razorblade, from the retinal periphery toward the optic nerve head (see Fig. 6).

Antibodies

Primary and secondary antibody concentrations were the same for both whole-mount preparations and vertical sections. All antibodies were diluted in blocking solution as described above. Primary antibodies were obtained from the following sources, and used at the following dilutions: anti-rabbit DARPP-32 (#2302, Cell Signaling; Beverly, MA), 1:100; monoclonal anti-parvalbumin clone Parv-19 (#P3088, Sigma Chemical, St. Louis, MO), 1:1000; monoclonal anti-tyrosine hydroxylase (#MAB318, Chemicon; Temecula, CA), 1:200. Secondary antibodies were species-specific anti-IgGs conjugated to Alexa Fluor 488, 555 or 594 (Molecular Probes; Eugene, OR) or Cy3 (Jackson Immuno Research; West Grove, PA) and were diluted 1:300. For multiple labeling, single sections were incubated in mixtures of primary antibodies, followed by mixtures of secondary antibodies, with the same intervening and subsequent steps as for single-antibody trials.

The blocking peptide used to test for the specificity of anti-DARPP-32 antibody binding was the synthetic peptide used to generate the anti-DARPP-32 antibody. This peptide was derived from the human DARPP-32 sequence, and was a generous gift from Dr. K.M. Sprott (Cell Signaling Technology; Beverly, MA).

Reagents

Reagents were obtained from the following sources: Abbott (Chicago, IL): sodium pentobarbital (#0074-378-05); Amersham Life Science (Cleveland, OH): glycerol (#56-81-5); Bio-Rad (Hercules, CA): Bradford reagent (#500-0006) and sodium dodecylsulfate (SDS; #161-0300); Calbiochem (San Diego, CA): FluorSave (#B34539); Fisher Scientific (Santa Clara, CA): Triton X-100 (#BP151-100) and bromophenol blue (#016426); GIBCO (Grand Island, NY): phosphate-buffered saline, Ca^{2+}- and Mg^{2+}-free, pH 7.4 (#70011-044); Invitrogen (Carlsbad, CA): Magic Mark (#LC5600); Jackson ImmunoResearch (West Grove, PA): normal goat serum (#005000121); Pierce (Rockford, IL): Blue Ranger (#26681) and SuperSignal West Pico Chemiluminescent Substrate (#34080); Roche (Indianapolis, IN): L-1-Chloro-3-(4-tosylamido)-4-phenyl-2butanone (TPCK; #874507), leupeptin (#1017101), pepstatin A (#253286), calpain I inhibitor (#1086090), calpain II inhibitor (#1086103); Sigma Chemical (St. Louis, MO): bovine serum albumin (BSA; #A7284), ethylenediamine tetraacetic acid (EDTA; #E6758), NaF (#S6521), beta glycerol phosphate (#G6376), sodium orthovanadate (#S6508), aprotinin (#A6279), benzamidine (#B6506), Tween 20 (# P9416), Ponceau S (#P7767); VWR (San Francisco, CA): O.C.T compound (#4583).

Imaging

Confocal images were obtained by excitation of the fluorescent dyes conjugated to the secondary antibodies. Images were collected with either an Olympus (Melville, NY) FluoView 300 or Bio-Rad (Hemel Hempstead, UK) Radiance 2100 Confocal System. The Olympus system used an Olympus IX70 inverted microscope, while the Bio-Rad system

was interfaced to an Olympus BX50WI upright microscope. Images were collected with either 40× or 60× oil immersion objectives. Excitation was provided by Ar (488 nm) and Kr (568 nm) lasers on the Olympus confocal and by multi-line Ar (488 nm used exclusively) and HeNe (543 nm) lasers on the Bio-Rad. Low magnification images of whole retinal preparations were obtained using epifluorescence on a Nikon Eclipse E1000 microscope with a 2X objective (0.1 n.a.; Nikon #93101). These images typically captured 10–25% of the entire retinal area, and were montaged together to produce pictures of the full flattened retinas in Adobe Illustrator (version 9.0.1, Adobe Systems, San Jose, CA).

When acquiring images of doubly-stained tissue, we would alternate between excitation wavelengths and adjust detector settings appropriately to minimize any signal arising from the other dye. Such “cross-talk” was not a problem when exciting with the longer-wavelength lasers (543 and 568 nm), but the 488 nm excitation could also elicit a signal from the longer wavelength dyes (especially Cy3, Alexa Fluor 555). This signal contamination was minimized by lowering the intensity of the 488 nm illumination and by optimal use of available filter sets, such that fluorescence from the longer wavelength dye made a negligible contribution in the 488 nm image, especially on the Bio-Rad, as shown in Figure 1. All confocal images presented in this work were obtained on the Bio-Rad except Figure 3, which utilized only a single dye.

Generally, images were acquired as a z-series of confocal optical sections that spanned the thickness of the tissue in vertical sections or the layer of interest in flat-mounted retinas. In some cases, selected consecutive optical sections were merged to form a single composite image. This was done as a maximum intensity z-projection in FluoView software or, more commonly, using the public domain program ImageJ (version 1.31o, developed at the U.S. National Institutes of Health and available on the Internet at http://rsb.info.nih.gov/ij/). Images due to each dye were kept separately, and any adjustments to brightness or contrast were applied uniformly to all the images in that z-series. Such manipulations were done, as most appropriate, in FluoView, ImageJ, or Photoshop (version 5.5, Adobe Systems, San Jose, CA). Changes in color space, if needed, were applied in ImageJ. Overlay images were generated in Photoshop.

To perform a nearest-neighbor analysis, we used the image of a field of cells in a flat-mounted retina stained with anti-DARPP-32 antibody. Cells were differentiated from background in ImageJ using the Adjust Threshold and Analyze Particles functions to set a minimum size and intensity for the fluorescent signal. This provided a map showing the outlines of DARPP-32-positive cells (inset, Fig. 7). This same analysis provided a calibrated center-point determination for each cell, and this was used to identify the nearest neighbor for each cell using a custom routine in Excel (version 2002, Microsoft, Redmond, WA). Cells for which the nearest neighbor could be outside the recorded image were not included. Histograms of this nearest neighbor analysis and Gaussian fits were generated in SigmaPlot (version 5.05, SPSS, Chicago, IL).

To show the spatial relationship of cells and processes that were immunopositive for DARPP-32 and tyrosine hydroxylase (TH), we entered consecutive optical sections produced on the Bio-Rad Radiance 2100 into the image-analysis program Volocity with the Visualization and Classification extension packages (version 2.6, Improvision, Coventry, UK). Volocity was then used to render three-dimensional reconstructions of selected DARPP-32-positive cells and associated TH-positive processes.

RESULTS

DARPP-32 is present in rat retina

The results presented here differ from those of a previous study of DARPP-32 in retinas (Meister et al., 1991) in terms of the species examined and the antibodies used. We therefore began this study by estimating the molecular weight of the protein bound by our antibody, and tested whether this binding is inhibited by the peptide sequence that the antiserum was directed against. For this purpose, retinas were homogenized and the soluble proteins electrophoretically separated on polyacrylamide gels. A well-focused protein band was stained in nitrocellulose blots of these gels by anti-DARPP-32 antibody (lane 3, Fig. 2B), and the molecular weight of this band was estimated to be 32–34 kD by comparison of the position of this band with those of molecular weight standards (e.g., lane 2, Fig. 2B). This staining was reduced below detectable levels by pre-incubating the anti-DARPP-32 antibody with a two-fold higher concentration of blocking peptide (lane 1, Fig. 2B). The molecular weight estimate provided by Figure 2 agrees with the range reported previously for rat retina and rat brain using different anti-DARPP-32 antibodies (Walaas et al., 1983; Hemmings et al., 1984a; Hemmings and Greengard 1986). This similarity makes it likely that the immunostaining of rat retina with a polyclonal antibody directed against human DARPP-32 described below is recognizing the same molecule detected previously by immunostaining of cat, monkey, and human retina using a monoclonal antibody directed against bovine DARPP-32 (Meister et al. 1991).

Localization of DARPP-32

The western blot data in Figure 2 show that a protein recognized by an anti-DARPP-32 antibody can be solubilized from rat retina. We therefore attempted to identify the cells that express this protein. As a first step, we took advantage of the laminar organization of cell bodies in retinas, and stained transretinal (“vertical”) cryosections with our anti-DARPP-32 antibody (Fig. 3). This antibody consistently stained somata in the inner nuclear layer, adjacent to the inner plexiform layer (Fig. 3A). As in the western blot data described above, this staining was reduced below detectable levels by the blocking peptide (Fig. 3B). By contrast, we did not observe DARPP-32-like immunoreactivity in photoreceptors, the middle layer of the inner nuclear layer, or the ganglion cell layer (Figs. 3, 4). For brevity, we will use hereafter the term “DARPP cells” to denote the inner nuclear layer cells that exhibit DARPP-32-like immunoreactivity.

DARPP cells in rat retina presented the following morphological properties. Their somata measured between ~5 and 9 μm (in flat-mounted retinas, as described below), and protruded slightly into the inner plexiform layer (IPL). An apical dendrite projected a few microns from these somata further into the IPL, sometimes reaching as far as the distal (sclerad) 10–20% of the IPL (Figs. 3, 4, 5). Immunopositive nodules were found sprinkled within the distal 20–25% and proximal 20% of the IPL (Figs. 4, 5). DARPP cells were observed in all of the retinas we examined (n=13), and, as described below in more detail, they were also found in all quadrants of these retinas. The immunopositive somata were generally separated from adjacent immunopositive somata by a distance corresponding to 1–2 cell bodies, although some immunopositive cells were found abutting each other (see Figs. 3, 4, 5).

The characteristics listed above are consistent with the possibility that DARPP-32 is contained in some amacrine cells. If these are a single morphological type, our results suggest that this is a relatively abundant amacrine cell that arborizes in both the distal and proximal IPL. Because these properties are displayed by the amacrine cell subtype known as AII (Kolb and Famiglietti 1974; MacNeil and Masland 1998), and because AII amacrine

cells are dopamine-sensitive (Hampson et al. 1992; Mills and Massey 1995), we proceeded to test the possibility that AII amacrine cells are DARPP cells.

Identification of AII cells as the DARPP-32 positive cell in vertical sections

The classic method for immunocytochemically identifying AII amacrine cells in rat retina is to stain them for parvalbumin (Wässle et al., 1993; Chun et al., 1993; Gàbriel and Witkovsky 1998; Feigenspan et al., 2001; Contini and Raviola 2003). We therefore double-labeled retinas for parvalbumin (PV) and DARPP-32, using secondary antibodies conjugated to chromophores that we could image with negligible cross-contamination (see Methods). The PV immunostaining was robust (Fig. 4B, false-color green), and it was absent in preparations stained with the secondary antibody only (not shown). This PV-like immunoreactivity was found in somata at the proximal edge of the inner nuclear layer, apical dendrites that extended as far as half-way into the IPL, and in small nodules at the distal and proximal levels of the IPL where AII amacrine cell dendrites are known to arborize (Kolb and Famiglietti 1974; Voigt and Wässle 1987). To test the possibility that DARPP cells contain PV, DARPP-32 immunolabeling of the same field (Fig. 4A, false-color red) was then superimposed on the image of the PV cells (Fig. 4C). In the superimposed image, cells appeared yellow if DARPP-32- and PV-like immunoreactivities colocalized within them, and cells appeared either red or green if they had detectable amounts of one, but not the other, immunoreactivity. Figure 4C shows that none of the amacrine cell somata were red, and that nodules in the distal and proximal layers of the IPL were yellow, in the superimposed images. This indicates that all of the DARPP cells, and DARPP-immunopositive processes in the distal and proximal IPL, in Figure 4A contained PV. We observed this staining pattern in all of the vertical sections we examined.

By contrast, we did find a relatively small number of green cells in the superimposed images of some fields (e.g., Fig. 5, at arrows), and thus found that not all PV cells contained DARPP. This is not necessarily surprising, because previous studies have concluded that PV cells in rat retina include more than one subtype of amacrine cell (Hamano et al 1990; Wässle et al., 1993). In agreement with previous studies (Wässle et al., 1993; Massey and Mills, 1999; see also Casini et al., 1995), at least two subtypes of green (PV only) cells were discernible in our flat-mounted preparations. As illustrated by the cells pointed out in Figure 5, and as described further below, some cells presented a weak PV signal, while others were intensely PV-positive.

PV and DARPP-32 co-localization in flat-mounted retinas

Because PV-containing amacrine cells are known to be present across all regions of the rat retina (Wässle et al., 1993), we next compared the distribution of DARPP cells and PV cells in flat-mounted retinas. For this purpose, we collected images of >200 DARPP and PV cells in each of several fields that we found to be flat, in the dorso-nasal, dorso-temporal, ventro-nasal, and ventro-temporal quadrants of each of these retinas. We collected images from a total of 18 fields of ca. 280 μm^2 each in a total of 4 retinas, and deliberately bleached the fields we imaged (by scanning several times with the maximum laser intensity) to have a record of the position of these fields relative to the optic nerve head (Fig. 6A). As reported by Wässle et al (1993), we found no large variation in the population density of PV cells across the rat retina, and therefore we made no attempt to map the population density of DARPP cells as a function of distance from the optic nerve head.

The appearance and spacing of the PV cells resembled those found in previous studies and in our vertically sectioned material (Fig. 4B). As shown by the high magnification image (Fig. 6B) of the field labeled 1 in Figure 6A, the PV somata appeared either rounded or ellipsoid, and were usually separated by distances about twice the diameter of single cells

(Endo et al., 1985; Hamano et al., 1990; Wässle et al. 1993). The somata were largely, but not entirely, homogenous in intensity (Wässle et al., 1993). In optical sections at the level of these somata, the cell margins were crisp, and the background staining was very low. We did not systematically section through the IPL to examine the dendrites of these somata. However, PV-positive processes, suggestive of those observed in vertical sections, could be seen in some of our whole-mount preparations (compare Figs. 4B and 6B).

Figure 6C shows the same field stained for DARPP-32. Cell margins are not as distinct as with PV, overall background staining is more pronounced, and intensity of the cell-associated signal is more uniform than with PV. Staining for both PV and DARPP-32 is confined to the inner retina beginning with the inner nuclear area, and as anticipated from our vertically sectioned material, no significant staining for either marker was found in the distal portion of our flat-mounted material (not shown).

When we overlay the images of anti-PV and anti-DARPP-32 staining (Fig. 6D), all the red, DARPP cells in the middle panel appeared yellow, indicating that they overlap with the PV cells seen in the left panel. Since these are confocal images drawn from the same depth in the tissue, the implication is that the DARPP-32 signal arises from the same cells as the PV signal. Although there are, therefore, no “red” cells in the overlay image, there are some “green” cells. There is a set of intensely-fluorescing and a less-numerous set of weakly-fluorescing cells (examples of each indicated by arrows, Fig. 6D). Examination of flat-mounted retinas thus corroborated both of the staining patterns found in vertical sections, in that all DARPP cells appeared to contain PV-like immunoreactivity, and some PV cells did not contain detectable levels of DARPP. The PV cells that colocalize with DARPP-32, tended to have intermediate PV staining. Lastly, we sampled all four quadrants of the retina for PV and DARPP-32 staining (as in Fig. 6A), with essentially equivalent results (not shown).

Nearest-neighbor analysis

Previous studies have shown that PV cells are not randomly distributed in rat and other retinas (Wässle et al., 1993; Casini et al., 1995). We therefore determined the nearest-neighbor distance for DARPP cells, as described in Methods. A histogram for the field of cells in Figure 6C is shown in Figure 7. The mean nearest neighbor distance is 9.8±2.2 μm (mean ± SD, n=159), and the median is 9.6 μm. A single Gaussian distribution gives a fair fit to the histogram in Figure 7.

We performed this sort of analysis on a sample section from each quadrant of four full retinas from four different animals. The horizontal and vertical axes of each retina were recorded at the time of enucleation. The between-animal variation was much greater than the between-sample variation in any one retina, and we could not detect any consistent correlation between the sample quadrant and relative values of our data. The closest mean nearest neighbor distance in any sample was 9.7 μm; the largest was 15.1 μm. The nearest-neighbor distance for the retina with the smallest average over all four quadrants was 10.1 μm, the largest was 13.8 μm, and the average for all four retinas was 11.6 μm. Similarly, the DARPP cell density over a retina varied from 2600/mm^2 to 5000/mm^2, with the average of all four retinas being 4000/mm^2. Thus, our data agree well with nearest-neighbor distances and cell densities reported previously (Wässle et al., 1993; Casini et al., 1995; Rice and Curran 2000; Lee et al., 2004).

Soma size

The soma size of the DARPP cells was estimated from their profiles, imaged with PV, in projected whole-mount images. This assured that we viewed the entire profile of each soma,

with distinct margins. Most cells were slightly ellipsoid in shape. For the data in Figure 6B, best ellipse fit outlines generated in ImageJ gave an average major axis of 7.8 μm and minor axis of 6.0 μm, with an average ratio of major:minor axis of 1.3. Using the area of the best fit ellipse to calculate the diameter of an equivalent circle gives an average soma diameter of 6.9 μm (± 0.6 μm, SD; n = 334). A similar analysis confined to the DARPP-32-negative cells found the average major axis dimension for strongly-stained, PV-positive cells was 8.4 μm, the minor axis was 6.8 μm, the ratio major:minor was 1.24, and the diameter of a circle of equivalent area was 7.5 μm (± 0.7 μm, SD; n = 24). This suggests that this class of PV-positive, DARPP-32-negative cell is slightly larger than the DARPP-32-positive cells, but we do not exclude the possibility that the difference is only apparent from the better resolution afforded by the more intense fluorescent staining of these cells. The DARPP-32-negative cells with weak PV staining were too dim to analyze with confidence.

Association of DARPP cells with TH processes

Tyrosine hydroxylase (TH) is the rate-limiting enzyme in the biosynthesis of catecholamines from L-tyrosine. In flat-mount views of rat retina, previous studies showed that the dendritic processes of TH-containing amacrine cells (i.e., “TH processes”) collar the somata of PV amacrine cells (Voigt and Wässle 1987). Figure 8 (top) shows a projected field of five optical sections (1.2 μm total optical depth) of a flat-mounted retina doubly-stained for TH and DARPP-32. A TH process can be seen in close proximity to most, if not all, of the DARPP-32-immunopositive somata (“DARPP somata”) in this field. Figure 8 (bottom) presents sequences of high-magnification confocal optical sections showing the relation of TH processes and DARPP somata for three selected cells (indicated A–C in Fig. 8, top). In serial optical sections, DARPP somata seemed to be surrounded, more or less, by TH processes. This is demonstrated in Figure 8 (bottom) by rotated 3D reconstructions of these same DARPP cells and their proximate TH processes. Most of the TH processes that bordered the DARPP somata tended to be co-planar (Fig. 8, cells A and B), i.e., DARPP somata were encircled by “rings” of TH processes (Pourcho 1982; Voigt and Wässle 1987; Kolb et al., 1990; Wässle et al., 1993; Casini et al., 1995). However, there were also numerous examples of more “basket”-like arrangements, where the reconstructions showed either strands of continuous TH processes, or numerous spots of TH processes, sandwiched between the vitread side of a DARPP soma and the rest of the inner plexiform layer (see IPL images, Fig. 8, cells B and C), in addition to processes arranged more or less like a necklace around the soma.

DISCUSSION

DARPP Cell Attributes

The results of this study support three conclusions about the nature of DARPP cells. First, we infer that AII amacrine cells in rat retina are DARPP cells because (*i*) DARPP cells contain PV; (*ii*) DARPP somata and processes occupy levels of the inner nuclear and inner plexiform layers that are characteristic of AII amacrine cells; (*iii*) the spatial distribution of DARPP somata resembles that reported for AII cells, in terms of average spacing, cell density, and presence in all quadrants; and (*iv*) DARPP somata are surrounded by TH processes (cf., Wässle et al., 1993; Chun et al., 1993; Gàbriel and Witkovsky 1998; Feigenspan et al., 2001; Contini and Raviola 2003; Lee et al., 2004; see also Casini et al., 1995; Strettoi and Masland 1996). Because all of the DARPP cells we observed were PV-immunopositive, and the nearest-neighbor distances between DARPP cells could be fitted by a single Gaussian distribution, the simplest interpretation of our results is that a single population of cells expresses both DARPP-32 and PV. These appeared to be a subset of the entire PV-positive amacrine cell population in our preparations because some PV cells showed no detectable levels of DARPP-32.

Second, if AII amacrine cells are DARPP cells, then our results provide the first evidence to our knowledge that a glycinergic interneuron expresses DARPP-32. This inference is based on the presence of glycine and the Glyt-1 glycine transporter in AII amacrine cells (Pourcho and Goebel 1985; Menger et al., 1998; Deng et al., 2001) and the glycine responses of ganglion cells that are postsynaptic to AII amacrine cells (Müller et al., 1988). It is too early to know if glycinergic cells that are both PV- and DARPP-32-immunopositive are unique to retina. Although glycine and PV have been colocalized in brainstem neurons (e.g., Aoki et al., 1990), it remains to be seen if these contain DARPP-32, and PV-containing inhibitory neurons in other brain regions have been found to contain GABA (e.g. Celio 1986; Jones and Hendry 1989; Freund 1989).

Third, our results are consistent with the possibility that DARPP-32 mediates the dopamine responses of some, but not all, retinal neurons. Like Meister et al. (1991), we found DARPP-32-like immunoreactivity in a subset of the most vitread somata in the inner nuclear layer, suggesting that DARPP-32 is present in some, but not all, amacrine cells. In the same preparations, we did not observe DARPP cells in the outer nuclear layer, the middle of the inner nuclear layer, or the ganglion cell layer, and we did not observe convincing or consistent DARPP staining of cells in the distal portion of the inner nuclear layer. Because dopamine receptors have been found in rat photoreceptor, bipolar, Müller, horizontal, and TH cells (Seki et al., 1991; Tran and Dickman 1992; Wagner et al., 1993; Biedermann et al., 1995; Veruki and Wässle 1996; Shulman and Fox 1996; Nguyen-Legros et al., 1996; Veruki 1997; Derouiche and Asan 1999), the exclusive presence of DARPP-32 in AII amacrine cells would imply that dopamine responses of some retinal neurons might take place without DARPP-32. Likewise, in species other than rat, there is a difference between sites of retinal DARPP immunoreactivity and the demonstrated locations of dopamine receptors. Meister et al (1991) found DARPP-immunoreactivity in processes surrounding cat photoreceptor somata, the distal inner nuclear layer of monkey and human retina, the amacrine cell layer of cat and monkey retina, and the optic fiber layer of cat, monkey, and human retina, whereas dopamine receptors have been found in monkey and human outer nuclear layer (Zarbin et al., 1986; Dearry et al 1991). In addition, synapses from TH cells onto non-AII amacrine cells and TH cells have been found in cat and monkey retina (Hokoç and Mariani 1987, 1988; Kolb et al., 1990), and one study has reported that TH cells synapse onto bipolar cells in the most distal sublamina of the monkey inner plexiform layer (Hokoç and Mariani 1987).

Generality

Our immunostaining results provide the first identification of a retinal cell subtype that expresses DARPP-32. Because AII amacrine cells are generally thought to receive dopaminergic input (Bloomfield and Dacheux 2001), it would be valuable to test the generality of our results by probing retinas of other species for DARPP-32. Aside from the possibility of staining AII amacrine cells, which other dopamine-sensitive cells might stain? We would expect to stain other cell classes as did Meister et al. (1991) yet, for the reasons given above, we would not expect to stain all dopamine-sensitive cells. Our finding that DARPP-32 colocalizes with PV in rat raises the possibility that DARPP-32 co-localizes with PV in other species. If so, it would not be surprising to find DARPP-32 in at least some of the non-AII types of cells that are labeled by anti-PV antibodies in, for example, sculpin, salamander, pigeon, owl, mouse, gerbil, ground squirrel, rabbit, cat, and monkey retina (Röhrenbeck et al., 1987; Gàbriel and Straznicky 1992; Martin and Grünert 1992; Sanna et al., 1993; Peichl and Gonzalez-Soriano 1994; Casini et al., 1995; Strettoi and Masland, 1996; Goebel and Pourcho 1997; Massey and Mills 1999; Haverkamp and Wässle, 2000; Wässle et al., 2000; Deng et al., 2001; Cuenca et al., 2002). Recently, we tested this possibility in rhesus macaque monkey retina, and found that the anti-DARPP-32 and anti-PV antibodies used in this study label horizontal cells (unpublished observations), consistent

with the presence of DARPP cells in the distal portion of the monkey inner nuclear layer reported by Meister et al. (1991) and the PV-immunoreactivity of monkey horizontal cells described by Röhrenbeck et al. (1987).

A number of studies have found that staining patterns achieved with anti-PV antibodies differ with developmental stage, staining protocols, and time of day (Endo et al., 1985; Uesugi et al., 1992; Sanna et al., 1992; Peichl and Gonzalez-Soriano 1994; Casini et al., 1998; Gàbriel et al., 2004). These observations suggest that PV and DARPP-32 co-localizations other than those we report here might be found in younger rats or retinas that are prepared in different ways. We therefore view the data presented here as evidence that adult rat AII amacrine cells contain DARPP-32, but we do not exclude the possibility that DARPP-32 is present in other amacrine cells or in other cell classes.

Function

One would naturally ask if colocalization of PV and DARPP-32 is of functional importance to AII amacrine cells. Previous studies have shown that threonine-34 of phospho-DARPP-32 can be dephosphorylated in brain by the calcium/calmodulin activated phosphatase "calcineurin" (King et al., 1984). If a similar mechanism dephosphorylates DARPP-32 in AII amacrine cells, then the ability of parvalbumin to buffer intracellular calcium ions (Berchtold et al., 2000) would tend to guard DARPP-32 from inactivation, if not increase DARPP-32 activation (cf. Nishi et al., 1997). This might be useful in the retina where dopamine is released continuously during daylight hours (e.g., Kolbinger et al., 1990) and where depolarization of AII amacrine cells raises intracellular Ca^{2+} levels (Haberman et al., 2003). However, this is not the only possibility, because dephosphorylation of brain DARPP-32 by another calcium-dependent protein phosphatase ("PP2A") relieves the antagonism produced by phosphorylation at threonine-75 (e.g., Nishi et al., 2002), and because some adenylate cyclases can be activated by increases in intracellular Ca^{2+} levels.

Because brain neuronal responses to dopamine are impaired in DARPP-32-knock-out mice (Fienberg et al., 1998), it is tempting to suggest that DARPP-32 might be critically important for dopamine responses in rat AII amacrine cells. The most well known of these is the uncoupling of their homologous gap junctions (Hampson et al., 1992; Mills and Massey 1995). If dopamine elevated cAMP levels in rat AII amacrine cells, one could postulate that the gap junctions are uncoupled by the action of a protein kinase A as in fish cone horizontal cells (Lasater and Dowling 1985; DeVries and Schwartz 1989) and as proposed for rabbit AII amacrine cells (Hampson et al., 1992), and that the dopamine receptors are D1-type (i.e., the type that elevate cytoplasmic cAMP levels). However, the dopamine response of AII amacrine cells is unlikely to be so simple in several respects. First, the presence of DARPP-32 implies that dopamine receptor activation can recruit a more complex set of intracellular events in AII amacrine cells, at least in rat, including changes in PKA activation and phosphatase inhibition. Secondly, previous studies have shown D2-type receptors but not D1-type receptors on rat PV cells and on cells resembling AII amacrine cells in profile (Veruki and Wässle 1996; Bjelke et al., 1996; Contini and Raviola 2003; see also Puopolo et al., 2001). Thirdly, conditions that release dopamine are still being explored (see Besharse and Iuvone 1992; Marc 1995; Bloomfield et al., 1997), and until these are established, it will be difficult to say when and how DARPP-32 is involved in AII amacrine cell function(s). Lastly, a report that dopamine modulates glutamate- and GABA-gated currents in AII amacrine cells (Veruki and Hartveit 1997) leaves open the possibilities that DARPP-32 is not involved in controlling electrical coupling among AII amacrine cells, and that DARPP-32 facilitates other dopamine responses in the retina.

Acknowledgments

This work was supported by NIH grant EY 08120 (to A.T.I.) and National Eye Institute Core grant P30 EY12576. The authors thank G. Adamson for use of the Pelco microwave oven, E. Raviola for advice on microwave fixation, K.M. Sprott for the anti-DARPP-32 antibody blocking peptide used in this study, A. Rodriguez-Contreras and F. Ventimiglia for advice on using the BioRad confocal system, E.G. Jones for use of the Nikon Eclipse microscope, A. Graziano for photographing our flat-mounted retinas at low magnification, and L.M. Chalupa for use of the Volocity software.

REFERENCES

Aoki E, Semba R, Seto-Ohshima A, Heizmann CW, Kashiwamata S. Coexistence of parvalbumin and glycine in the rat brainstem. Brain Res. 1990; 525:140–143. [PubMed: 2245319]

Berchtold MW, Brinkmeier H, Münterner M. Calcium ion in skeletal muscle: Its crucial role for muscle function, plasticity, and disease. Physiol Rev. 2000; 80:1215–1265. [PubMed: 10893434]

Besharse JC, Iuvone PM. Is dopamine a light-adaptive or a dark-adaptive modulator in retina? Neurochem Int. 1992; 20:193–199. [PubMed: 1304858]

Biedermann B, Frohlich E, Grosche J, Wagner HJ, Reichenbach A. Mammalian Muller (glial) cells express functional D2 dopamine receptors. Neuroreport. 1995; 6:609–612. [PubMed: 7605910]

Bjelke B, Goldstein M, Tinner B, Andersson C, Sesack SR, Steinbusch HW, Lew JY, He X, Watson S, Tengroth B, Fuxe K. Dopaminergic transmission in the rat retina: evidence for volume transmission. J Chem Neuroanat. 1996; 12:37–50. [PubMed: 9001947]

Bloomfield SA, Dacheux RF. Rod vision: pathways and processing in the mammalian retina. Prog Retin Eye Res. 2001; 20:351–384. [PubMed: 11286897]

Bloomfield SA, Xin D, Osborne T. Light-induced modulation of coupling between AII amacrine cells in the rabbit retina. Vis Neurosci. 1997; 14:565–576. [PubMed: 9194323]

Brecha, N. Retinal neurotransmitters: Histochemical and biochemical studies. In: Emson, PC., editor. Chemical Neuroanatomy. New York: Raven Press; 1983. p. 85-129.

Casini G, Rickman DW, Brecha NC. AII amacrine cell population in the rabbit retina: identification by parvalbumin immunoreactivity. J Comp Neurol. 1995; 356:132–142. [PubMed: 7629307]

Casini G, Rickman DW, Trasarti L, Brecha NC. Postnatal development of parvalbumin immunoreactive amacrine cells in the rabbit retina. Brain Res Dev Brain Res. 1998; 111:107–117.

Celio MR. Parvalbumin in most gamma-aminobutyric acid-containing neurons of the rat cerebral cortex. Science. 1986; 231:995–997. [PubMed: 3945815]

Chun MH, Han SH, Chung JW, Wässle H. Electron microscopic analysis of the rod pathway of the rat retina. J Comp Neurol. 1993; 332:421–432. [PubMed: 8349841]

Contini M, Raviola E. GABAergic synapses made by a retinal dopaminergic neuron. Proc Natl Acad Sci U S A. 2003; 100:1358–1363. [PubMed: 12547914]

Cuenca N, Deng P, Linberg KA, Lewis GP, Fisher SK, Kolb H. The neurons of the ground squirrel retina as revealed by immunostains for calcium binding proteins and neurotransmitters. J. Neurocytol. 2002; 31:649–666. [PubMed: 14501205]

Dearry A, Falardeau P, Shores C, Caron MG. D2 dopamine receptors in the human retina: cloning of cDNA and localization of mRNA. Cell Mol Neurobiol. 1991; 11:437–453. [PubMed: 1835903]

Deng P, Cuenca N, Doerr T, Pow DV, Miller R, Kolb H. Localization of neurotransmitters and calcium binding proteins to neurons of salamander and mudpuppy retinas. Vision Res. 2001; 41:1771–1783. [PubMed: 11369041]

Derouiche A, Asan E. The dopamine D2 receptor subfamily in rat retina: ultrastructural immunogold and in situ hybridization studies. Eur J Neurosci. 1999; 11:1391–1402. [PubMed: 10103134]

DeVries SH, Schwartz EA. Modulation of an electrical synapse between solitary pairs of catfish horizontal cells by dopamine and second messengers. J Physiol. 1989; 414:351–375. [PubMed: 2558170]

Dowling JE. Retinal neuromodulation: the role of dopamine. Vis Neurosci. 1991; 7:87–97. [PubMed: 1718402]

Ehinger B. Functional role of dopamine in the retina. Progr Retina Res. 1983; 2:213–232.

Endo T, Kobayashi S, Onaya T. Parvalbumin in rat cerebrum, cerebellum and retina during postnatal development. Neurosci Lett. 1985; 60:279–282. [PubMed: 3906443]

Feigenspan A, Teubner B, Willecke K, Weiler R. Expression of neuronal connexin36 in AII amacrine cells of the mammalian retina. J Neurosci. 2001; 21:230–239. [PubMed: 11150340]

Fienberg AA, Hiroi N, Mermelstein PG, Song W, Snyder GL, Nishi A, Cheramy A, O'Callaghan JP, Miller DB, Cole DG, Corbett R, Haile CN, Cooper DC, Onn SP, Grace AA, Ouimet CC, White FJ, Hyman SE, Surmeier DJ, Girault J, Nestler EJ, Greengard P. DARP-32: Regulator of the efficacy of dopaminergic neurotransmission. Science. 1998; 281:838–842. [PubMed: 9694658]

Freund TF. GABAergic septohippocampal neurons contain parvalbumin. Brain Res. 1989; 478:375–381. [PubMed: 2924136]

Gàbriel R, Lesauter J, Banvolgyi T, Petrovics G, Silver R, Witkovsky P. AII amacrine neurons of the rat retina show diurnal and circadian rhythms of parvalbumin immunoreactivity. Cell Tissue Res. 2004; 315:181–186. [PubMed: 14610664]

Gàbriel R, Straznicky C. Immunocytochemical localization of parvalbumin- and neurofilament triplet protein immunoreactivity in the cat retina: colocalization in a subpopulation of AII amacrine cells. Brain Res. 1992; 595:133–136. [PubMed: 1467949]

Gàbriel R, Witkovsky P. Cholinergic, but not the rod pathway-related glycinergic (All), amacrine cells contain calretinin in the rat retina. Neurosci Lett. 1998; 247:179–182. [PubMed: 9655622]

Goebel DJ, Pourcho RG. Calretinin in the cat retina: colocalizations with other calcium-binding proteins, GABA and glycine. Vis Neurosci. 1997; 14:311–322. [PubMed: 9147483]

Greengard P, Allen PB, Nairn AC. Beyond the dopamine receptor: the DARPP-32/protein phosphatase-1 cascade. Neuron. 1999; 23:435–447. [PubMed: 10433257]

Gustincich S, Feigenspan A, Sieghart W, Raviola E. Composition of the GABA(A) receptors of retinal dopaminergic neurons. J Neurosci. 1999; 19:7812–7822. [PubMed: 10479684]

Habermann CJ, O'Brien BJ, Wassle H, Protti DA. AII amacrine cells express L-type calcium channels at their output synapses. J Neurosci. 2003; 23:6904–6913. [PubMed: 12890785]

Häggendal J, Malmfors T. Identification and cellular localization of the catecholamines in the retina and the choroid of the rabbit. Acta Physiol Scand. 1965; 64:58–66. [PubMed: 14348505]

Hamano K, Kiyama H, Emson PC, Manabe R, Nakauchi M, Tohyama M. Localization of two calcium binding proteins, calbindin (28 kD) and parvalbumin (12 kD), in the vertebrate retina. J Comp Neurol. 1990; 302:417–424. [PubMed: 2289978]

Hampson EC, Vaney DI, Weiler R. Dopaminergic modulation of gap junction permeability between amacrine cells in mammalian retina. J Neurosci. 1992; 12:4911–4922. [PubMed: 1281499]

Haverkamp S, Wässle H. Immunocytochemical analysis of the mouse retina. J Comp Neurol. 2000; 424:1–23. [PubMed: 10888735]

Hemmings HC, Nairn AC, Aswad DW, Greengard P. DARPP-32, a dopamine- and adenosine 3’:5’-monophosphate-regulated phosphoprotein enriched in dopamine-innervated brain regions. II. Purification and characterization of the phosphoprotein from bovine caudate nucleus. J Neurosci. 1984a; 4:99–110. [PubMed: 6319628]

Hemmings HC Jr, Nairn AC, Greengard P. DARPP-32, a dopamine- and adenosine 3':5'-monophosphate-regulated neuronal phosphoprotein. II. Comparison of the kinetics of phosphorylation of DARPP-32 and phosphatase inhibitor 1. J Biol Chem. 1984b; 259:14491–14497. [PubMed: 6501303]

Hemmings HC, Greengard P. DARPP-32, a dopamine- and adenosine 3’:5’-monophosphate-regulated phosphoprotein: Regional, tissue, and phylogenetic distribution. J Neurosci. 1986; 6:1469–1481. [PubMed: 3711991]

Hokoç JN, Mariani AP. Tyrosine hydroxylase immunoreactivity in the rhesus monkey retina reveals synapses from bipolar cells to dopaminergic amacrine cells. J Neurosci. 1987; 7:2785–2793. [PubMed: 2887643]

Hokoç JN, Mariani AP. Synapses from bipolar cells onto dopaminergic amacrine cells in cat and rabbit retinas. Brain Res. 1988; 461:17–26. [PubMed: 2906268]

Jones EG, Hendry SH. Differential calcium binding protein immunoreactivity distinguishes classes of relay neurons in monkey thalamic nuclei. Eur J Neurosci. 1989; 1989:222–246. [PubMed: 12106154]

King MM, Huang CY, Chock PB, Nairn AC, Hemmings HC, Chan K-FJ, Greengard P. Mammalian brain phosphoproteins as substrates for calcineurin. J Biol Chem. 1984; 259:8080–8083. [PubMed: 6330098]

Kolb H, Cuenca N, Wang HH, Dekorver L. The synaptic organization of the dopaminergic amacrine cell in the cat retina. J Neurocytol. 1990; 19:343–366. [PubMed: 2391538]

Kolb H, Famiglietti EV. Rod and cone pathways in the inner plexiform layer of the cat retina. Science. 1974; 186:47–49. [PubMed: 4417736]

Kolbinger W, Kohler K, Oetting H, Weiler R. Endogenous dopamine and cyclic events in the fish retina, I: HPLC assay of total content, release, and metabolic turnover during different light/dark cycles. Vis Neurosci. 1990; 5:143–149. [PubMed: 2278941]

Lasater EM, Dowling JE. Dopamine decreases conductance of the electrical junctions between cultured retinal horizontal cells. Proc Natl Acad Sci U S A. 1985; 82:3025–3029. [PubMed: 3857632]

Lee E-J, Kim H-J, Lim E-J, Kim I-B, Kang W-S, Oh S-J, Rickman DW, Chung J-W, Chun M-H. AII amacrine cells in the mammalian retina show Disabled-1 immunoreactivity. J Comp Neurol. 2004; 470:372–381. [PubMed: 14961563]

MacNeil MA, Masland RH. Extreme diversity among amacrine cells: Implications for function. Neuron. 1998; 20:971–982. [PubMed: 9620701]

Malmfors T. Evidence of adrenergic neurons with synaptic terminals in the retina of rats demonstrated with fluorescence and electron microscopy. Acta Physiol Scand. 1963; 58:99–100. [PubMed: 13932601]

Marc, RE. Interplexiform cell connectivity in the outer retina. In: Djamgoz, MBA.; Archer, SN.; Vallerga, S., editors. Neurobiology and Clinical Aspects of the Outer Retina. London: Chapman & Hall; 1995. p. 369-393.

Martin PR, Grünert U. Spatial density and immunoreactivity of bipolar cells in the macaque monkey retina. J Comp Neurol. 1992; 323:269–287. [PubMed: 1401260]

Massey SC, Mills SL. Antibody to calretinin stains AII amacrine cells in the rabbit retina: Double-label and confocal analyses. J Comp Neurol. 1999; 411:3–18. [PubMed: 10404104]

Meister B, Arvidsson U, Hemmings HC Jr, Greengard P, Hokfelt T. Dopamine- and adenosine-3':5'-monophosphate (cAMP)-regulated phosphoprotein of Mr 32,000 (DARPP-32) in the retina of cat, monkey and human. Neurosci Lett. 1991; 131:66–70. [PubMed: 1791981]

Menger N, Pow DV, Wässle H. Glycinergic amacrine cells of the rat retina. J Comp Neurol. 1998; 401:34–46. [PubMed: 9802699]

Mills SL, Massey SC. Differential properties of two gap junctional pathways made by AII amacrine cells. Nature. 1995; 377:734–737. [PubMed: 7477263]

Müller F, Wässle H, Voigt T. Pharmacological modulation of the rod pathway in the cat retina. J Neurophysiol. 1988; 59:1657–1672. [PubMed: 3404200]

Nishi A, Snyder GL, Greengard P. Bidirectional regulation of DARPP-32 phosphorylation by dopamine. J Neurosci. 1997; 17:8147–8155. [PubMed: 9334390]

Nishi A, Bibb JA, Matsuyama S, Hamada M, Higashi H, Nairm AC, Greengard P. Regulation of DARPP-32 dephosphorylation at PKA- and Cdk5-sites by NMDA and AMPA receptors: distinct roles of calcineurin and protein phosphatase-2A. J Neurochem. 2002; 81:832–841. [PubMed: 12065642]

Nishi A, Bibb JA, Snyder GL, Higashi H, Nairn AC, Greengard P. Amplification of dopaminergic signaling by a positive feedback loop. Proc Natl Acad Sci USA. 2000; 97:12840–12845. [PubMed: 11050161]

Nguyen-Legros J, Chanut E, Versaux-Botteri C, Simon A, Trouvin JH. Dopamine inhibits melatonin synthesis in photoreceptor cells through a D2-like receptor subtype in the rat retina: biochemical and histochemical evidence. J Neurochem. 1996; 67:2514–2520. [PubMed: 8931485]

Patel S, Chapman KL, Marston D, Hutson PH, Ragan CI. Pharmacological and functional characterisation of dopamine D4 receptors in the rat retina. Neuropharmacol. 2003; 44:1038–1046.

Peichl L, Gonzalez-Soriano J. Morphological types of horizontal cell in rodent retinae: a comparison of rat, mouse, gerbil, and guinea pig. Vis Neurosci. 1994; 11:501–517. [PubMed: 8038125]

Pourcho R. Dopaminergic amacrine cells in the cat retina. Brain Res. 1982; 252:101–109. [PubMed: 7172014]

Pourcho RG, Goebel DJ. A combined Golgi and autoradiographic study of (3H)glycine-accumulating amacrine cells in the cat retina. J Comp Neurol. 1985; 233:473–480. [PubMed: 2984258]

Puopolo M, Hochstetler SE, Gustincich S, Wightman RM, Raviola E. Extrasynaptic release of dopamine in a retinal neuron: activity dependence and transmitter modulation. Neuron. 2001; 30:211–225. [PubMed: 11343656]

Pycock CJ, Smith LFP. Interactions of dopamine and the release of [3H]-taurine and [3H]-glycine from the isolated retina of the rat. Br J Pharmacol. 1983; 78:395–404. [PubMed: 6187404]

Rice DS, Curran T. Disabled-1 is expressed in type AII amacrine cells in the mouse retina. J Comp Neurol. 2000; 424:327–338. [PubMed: 10906706]

Röhrenbeck J, Wässle H, Heizmann CW. Immunocytochemical labelling of horizontal cells in mammalian retina using antibodies against calcium binding proteins. Neurosci Lett. 1987; 77:255–260. [PubMed: 3302765]

Sanna PP, Keyser KT, Celio MR, Karten HJ, Bloom FE. Distribution of parvalbumin immunoreactivity in the vertebrate retina. Brain Res. 1993; 600:141–150. [PubMed: 8422581]

Sanna PP, Keyser KT, Deerink TJ, Ellisman MH, Karten HJ, Bloom FE. Distribution and ontogeny of parvalbumin immunoreactivity in the chicken retina. Neurosci. 1992; 47:745–751.

Schiffmann SN, Lledo PM, Vincent JD. Dopamine D1 receptor modulates the voltage-gated sodium current in rat striatal neurones through a protein kinase A. J Physiol. 1995; 483:95–107. [PubMed: 7776243]

Schiffmann SN, Desdouits F, Menu R, Greengard P, Vincent JD, Vanderhaeghen JJ, Girault JA. Modulation of the voltage-gated sodium current in rat striatal neurons by DARPP-32, an inhibitor of protein phosphatase. Eur J Neurosci. 1998; 10:1312–1320. [PubMed: 9749785]

Seki T, Fukado S, Shioda S, Nakai Y, Koide R, Fukado Y. Immunoelectron microscopic observation of cells in the rat retinal containing gamma-aminobutyric acid and catecholamine. Jpn J Ophthalmol. 1991; 35:30–41. [PubMed: 1895567]

Shulman LM, Fox DA. Dopamine inhibits mammalian photoreceptor Na^+,K^+-ATPase activity via a selective effect on the α3 isozyme. Proc Natl Acad Sci U S A. 1996; 93:8034–8039. [PubMed: 8755598]

Strettoi E, Masland RH. The number of unidentified amacrine cells in the mammalian retina. Proc Natl Acad Sci U S A. 1996; 93:14906–14911. [PubMed: 8962154]

Surmeier DJ, Bargas J, Hemmings HC Jr, Nairn AC, Greengard P. Differential modulation of calcium currents by the D1 dopaminergic signaling pathway in rat neostriatal neurons. Neuron. 1994; 14:385–397. [PubMed: 7531987]

Tran VT, Dickman M. Differential localization of dopamine D1 and D2 receptors in rat retina. Invest Ophthalmol Vis Sci. 1992; 33:1620–1626. [PubMed: 1532792]

Uesugi R, Yamada M, Mizuguchi M, Baimbridge KG, Kim SU. Calbindin D-28k and parvalbumin immunohistochemistry in developing rat retina. Exp Eye Res. 1992; 54:491–499. [PubMed: 1623935]

Veruki ML. Dopaminergic neurons in the rat retina express dopamine D2/3 receptors. Eur J Neurosci. 1997; 9:1096–1100. [PubMed: 9182963]

Veruki ML, Hartveit E. Ligand-gated currents of AII amacrine cells in the rat retina and their modulation by dopamine. Society for Neuroscience Abstracts. 1997; 23:450.

Veruki ML, Wässle H. Immunohistochemical localization of dopamine D1 receptors in rat retina. Eur J Neurosci. 1996; 8:2286–2297. [PubMed: 8950093]

Voigt T, Wässle H. Dopaminergic innervation of A II amacrine cells in mammalian retina. J Neurosci. 1987; 7:4115–4128. [PubMed: 2891802]

Wagner HJ, Luo BG, Ariano MA, Sibley DR, Stell WK. Localization of D2 dopamine receptors in vertebrate retinae with anti-peptide antibodies. J Comp Neurol. 1993; 331:469–481. [PubMed: 8509505]

Walaas SI, Aswad DW, Greengard P. A dopamine- and cyclic AMP-regulated phosphoprotein enriched in dopamine-innervated brain regions. Nature. 1983; 301:69–71. [PubMed: 6296685]

Wässle H, Dacey DM, Haun T, Haverkamp S, Grünert U, Boycott BB. The mosaic of horizontal cells in the macaque monkey retina: With a comment on biplexiform ganglion cells. Vis Neurosci. 2000; 17:591–608. [PubMed: 11016578]

Wässle H, Grunert U, Röhrenbeck J. Immunocytochemical staining of AII-amacrine cells in the rat retina with antibodies against parvalbumin. J Comp Neurol. 1993; 332:407–420. [PubMed: 8349840]

Witkovsky P, Dearry A. Functional roles of dopamine in the vertebrate retina. Prog Retina Res. 1991; 11:247–292.

Yan Z, Hsieh-Wilson L, Feng J, Tomizawa K, Allen PB, Fienberg AA, Nairn AC, Greengard P. Protein phosphatase 1 modulation of neostriatal AMPA channels: regulation by DARPP-32 and spinophilin. Nature Neurosci. 1999; 2:13–17. [PubMed: 10195174]

Zarbin MA, Wamsley JK, Palacios JM, Kuhar MJ. Autoradiographic localization of high affinity GABA, benzodiazepine, dopaminergic, adrenergic and muscarinic cholinergic receptors in the rat, monkey and human retina. Brain Res. 1986; 374:75–92. [PubMed: 3013364]

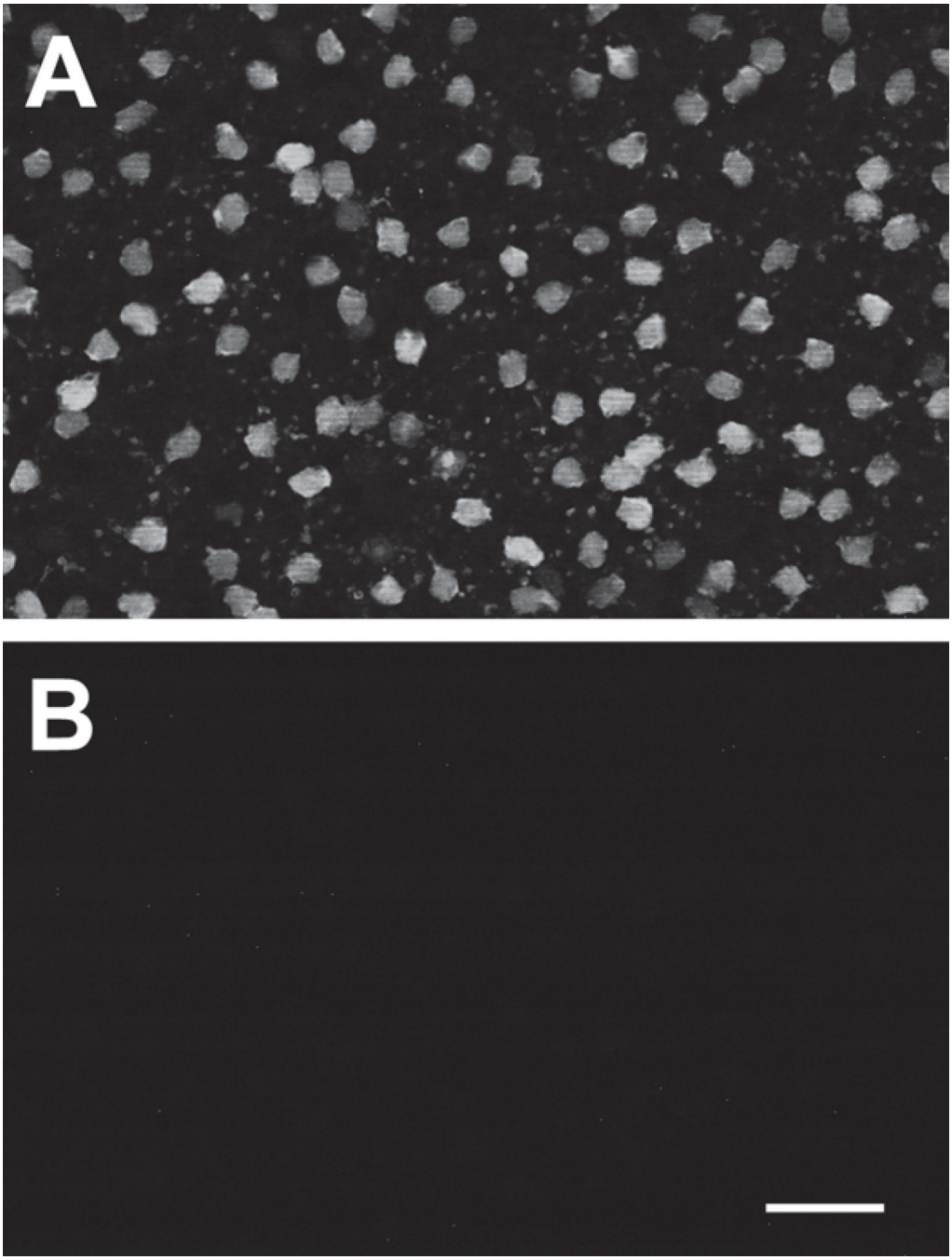

Figure 1.

Cross-signal contamination was very low. Flat-mounted retina labeled with anti-parvalbumin antibody and visualized with Alexa Fluor 488-conjugated secondary antibody, as described for Figures 4, 5, and 6. **(A)** Normal image optimized to capture the signal generated by the 488 dye. **(B)** The exact same field obtained with 488 illumination but using the settings and filter sets normally used to acquire the image generated by secondary antibodies conjugated to cy3, Alexa Fluor 555 or Alexa Fluor 594. Scale bar is 25 μm. No cross-signal contamination is visible at these settings. If brightness and contrast are greatly increased, a signal on the order of 1% of panel **A** can be seen (not shown). Images of all

double-labeled preparations were used for data analysis only if cross-signal contamination was as low as shown here.

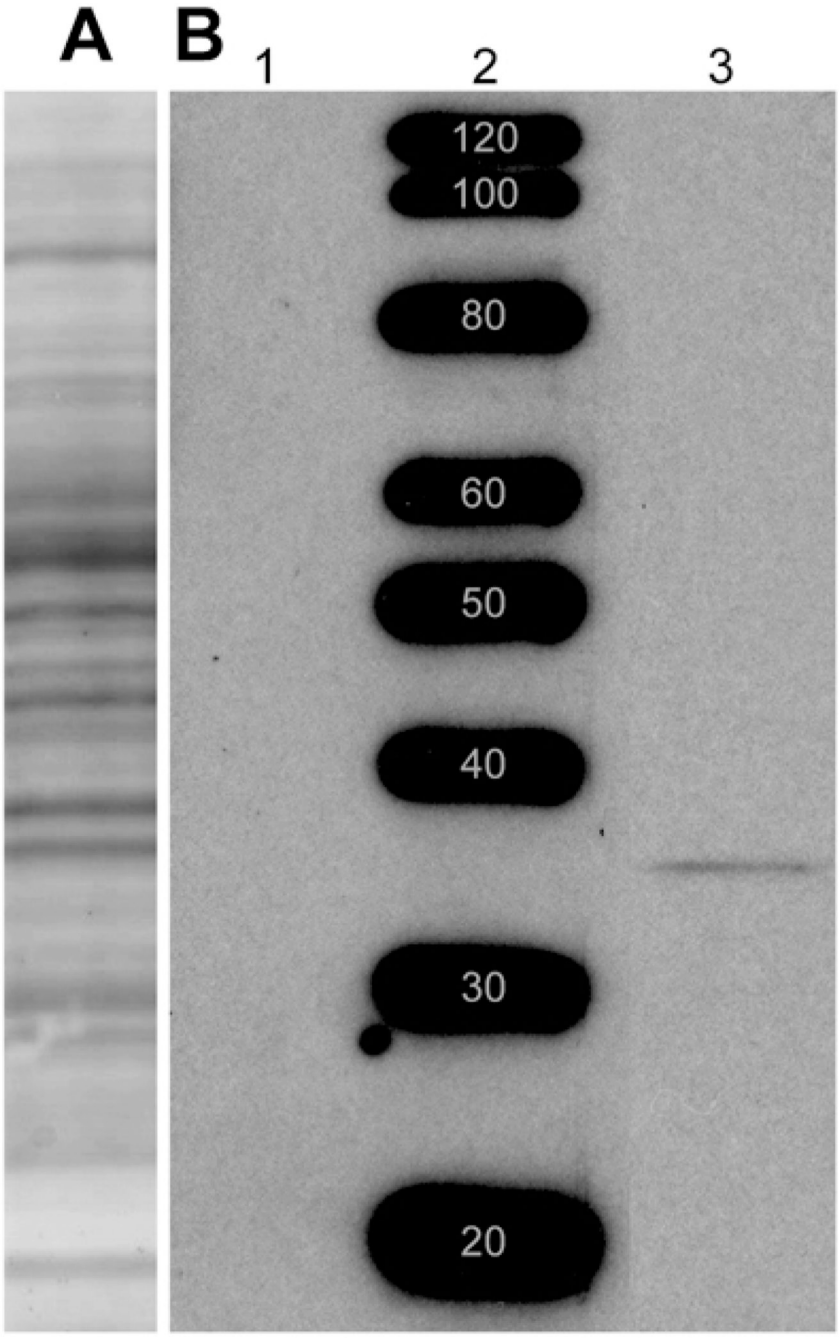

Figure 2.

Western Blot: 100-µg samples of rat retina lysate and protein standards were resolved by electrophoresis and transferred onto nitrocellulose. (**A**) Ponceau S probe of a single lane of retina lysate shows that multiple protein bands transferred from the gel to the nitrocellulose. The positions of molecular weight standard proteins run adjacent to this lane are identical to those in **B** and, therefore, not shown. (**B**) Specific DARPP-32 staining: Retina lysate samples were run in lanes 1 and 3, on either side of a lane of molecular weight standard proteins. Lane 3 was probed with anti-DARPP-32 antibody, while lane 1 was probed with anti-DARPP-32 antibody that had been pre-incubated overnight with blocking peptide. Anti-DARPP-32 antibody stained a well-focused protein band in lane 3, and this staining was

blocked completely by the antibody blocking peptide (lane 1). The molecular weight of this band was estimated to be 32 kD, by comparison with a standard curve constructed from the distances migrated by the protein standards (lane 2). Note that the blot in **B** was prepared from a different gel than the blot in **A**. Blot in **A** included to show typical range of proteins obtained from retinal homogenates. Bands in **B**, lane 2, are prominent because Magic Mark standards have been optimized for visualization with HRP.

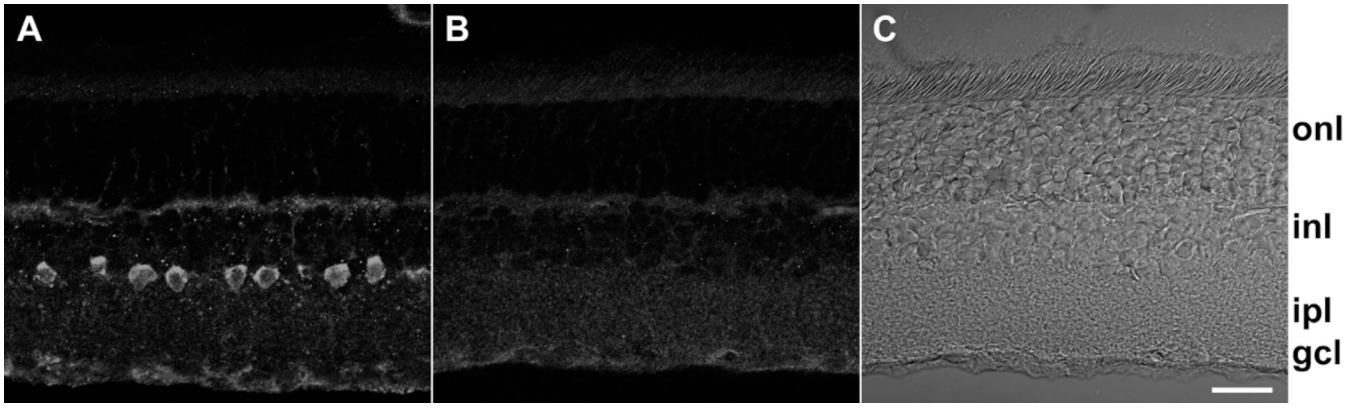

Figure 3.

Localization of DARPP-32 in vertical sections. **(A)** Labeling with anti-DARPP-32 antibody visualized with Alexa Fluor 555-conjugated anti-rabbit IgG. Confocal images were obtained at 0.25 μm z intervals with 3-frame Kalman averaging on the Olympus FluoView 300. This image is the result of a maximum intensity z-projection of 2 consecutive optical sections from the middle of this series. **(B)** Exactly the same protocol and conditions as **A** and performed on the same day, except that this section was incubated with primary anti-DARPP-32 antibody that had been pre-incubated overnight with anti-DARPP-32 antibody blocking peptide. This image is a z-projection of 3 consecutive optical sections. **(C)** The corresponding DIC image for panel **B**. Labels along right side indicate position of outer nuclear layer ("onl"), inner nuclear layer ("inl"), inner plexiform layer ("ipl"), ganglion cell layer ("gcl"). **A, B**, and **C** displayed at identical magnifications. Scale bar is 20 μm.

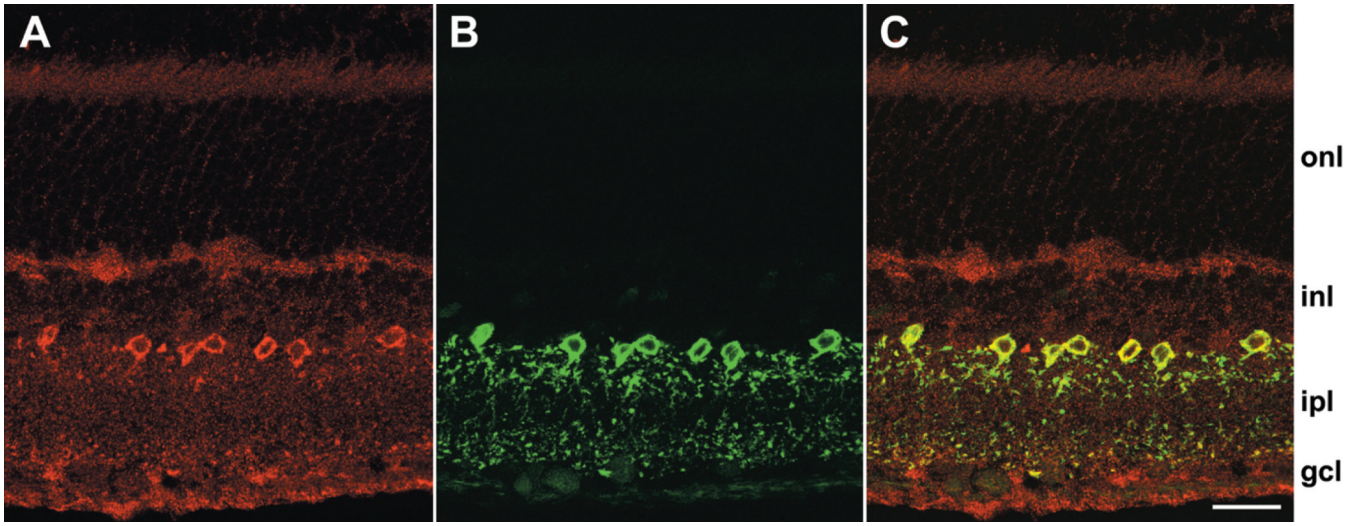

Figure 4.

Colocalization of parvalbumin and DARPP-32 in vertical sections. (**A**) Labeling with anti-DARPP-32 antibody visualized with cy3-conjugated anti-rabbit IgG. Confocal images were obtained at 0.20 μm z intervals with 3-frame Kalman averaging on the Bio-Rad Radiance 2100. This image is the result of a maximum intensity z-projection of 6 consecutive optical sections. (**B**) Labeling with anti-parvalbumin antibody visualized with Alexa Fluor 488-conjugated anti-mouse IgG. These data were obtained concurrently with the anti-DARPP-32 images in panel **A** using Sequential acquisition mode, in which fluorescence due to each dye is obtained individually. (**C**) Direct overlay of panels **A** and **B**. Yellow indicates regions of overlapping red and green signal. Position of retinal layers indicated as in Figure 3. Scale bar is 20 μm.

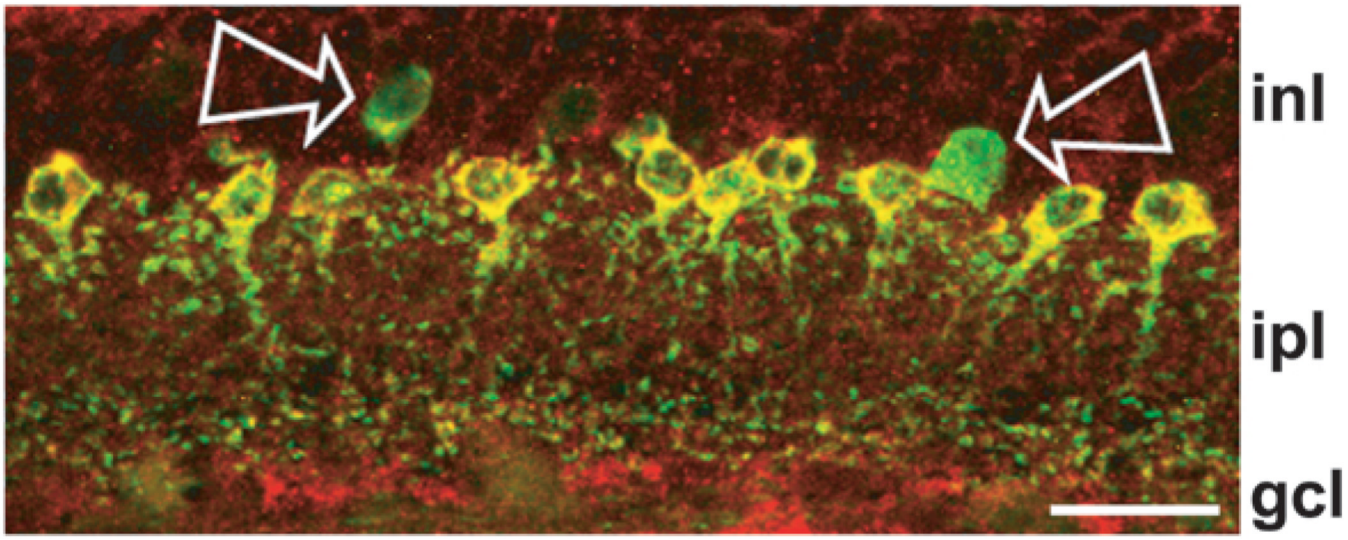

Figure 5.

Parvalbumin, without detectable DARPP-32, in some cells in vertical sections. Direct overlay of PV and DARPP-32 immunolabeling of a field imaged as in Figure 4, except that DARPP-32 was visualized with Alexa Fluor 594-conjugated secondary and the image is a z-projection of 5 optical sections obtained at 0.30 μm z intervals with 2-frame Kalman averaging. Yellow indicates regions of overlapping red and green signal. Arrows show two cells that were PV positive and DARPP-32 negative. Note that one of these fluoresced weakly (left arrow), while the other fluoresced brightly (right arrow). Position of retinal layers indicated as in Figure 4. Scale bar is 20 μm.

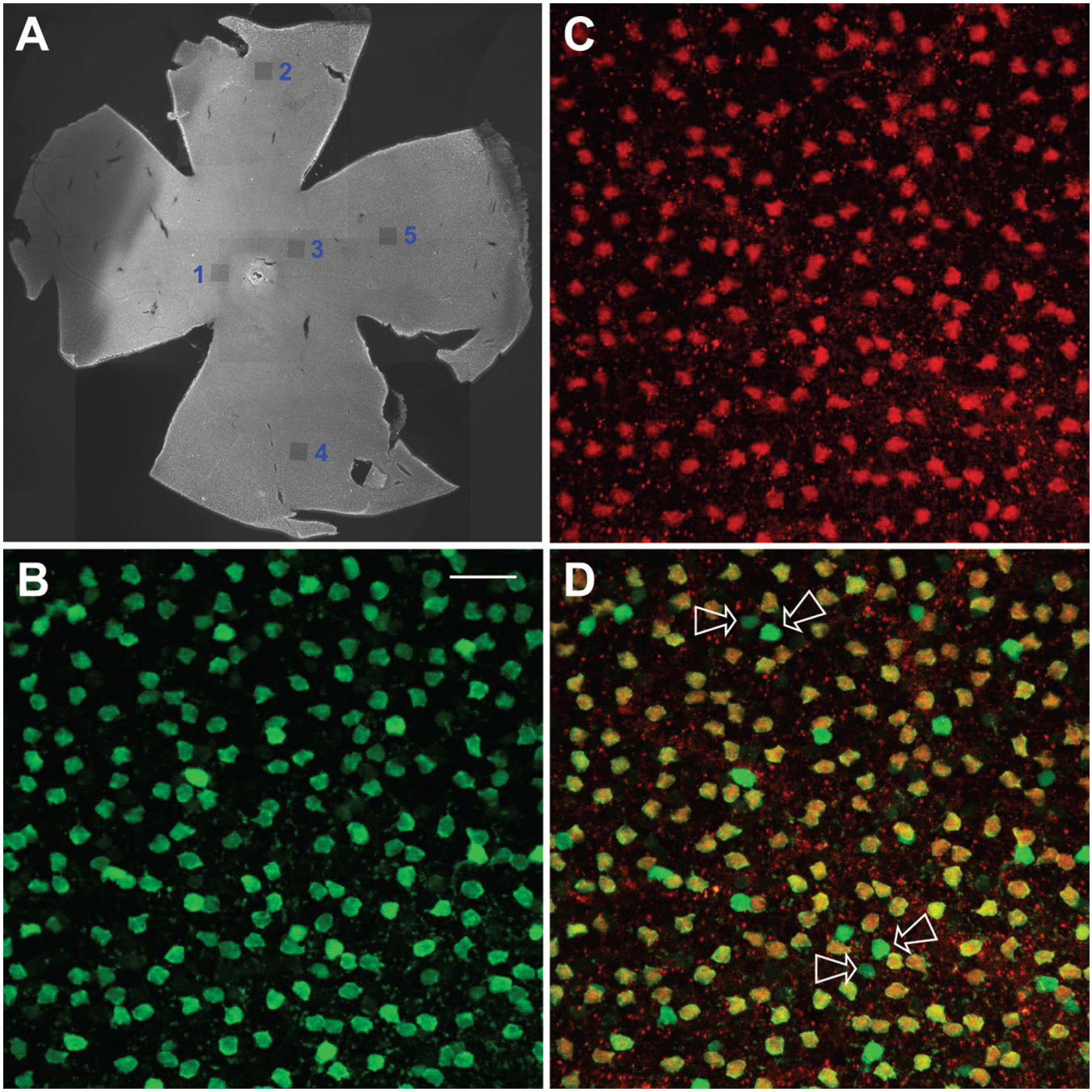

Figure 6.

Colocalization of parvalbumin and DARPP-32 in whole retina. (**A**) Epi-fluorescence low-magnification image of an entire flattened retina. This tissue was probed with anti-PV and anti-DARPP-32 antibodies and counterstained with Alexa Fluor 488 for PV and Alexa Fluor 555 for DARPP-32. The small, darkened squares, numbered 1–5, are areas that were imaged at higher magnification on the Bio-Rad Radiance 2100 and then deliberately bleached by exposure to the Ar 488 laser line at full power. The optic nerve head is whitish in this image, and can be seen part way between the areas numbered 1 and 3. The false-color fluorescent images in **B–D** were taken from the area labeled “1”, which was in the dorsal-temporal region of this retina. (**B**) PV-positive cells. Confocal images obtained at 0.30 μm z intervals

with 2-frame Kalman averaging. This is a maximum intensity z-projection of 9 consecutive optical sections. (**C**) DARPP-32-positive cells. Same conditions as panel **B**. (**D**) Overlay of panels **B** and **C**. Yellow indicates regions of overlapping red and green signal. Arrows show some of the cells that were PV positive and DARPP-32 negative. Note that, between each pair of arrows, one of these fluoresced weakly, while the other fluoresced brightly. Scale bar is 25 μm.

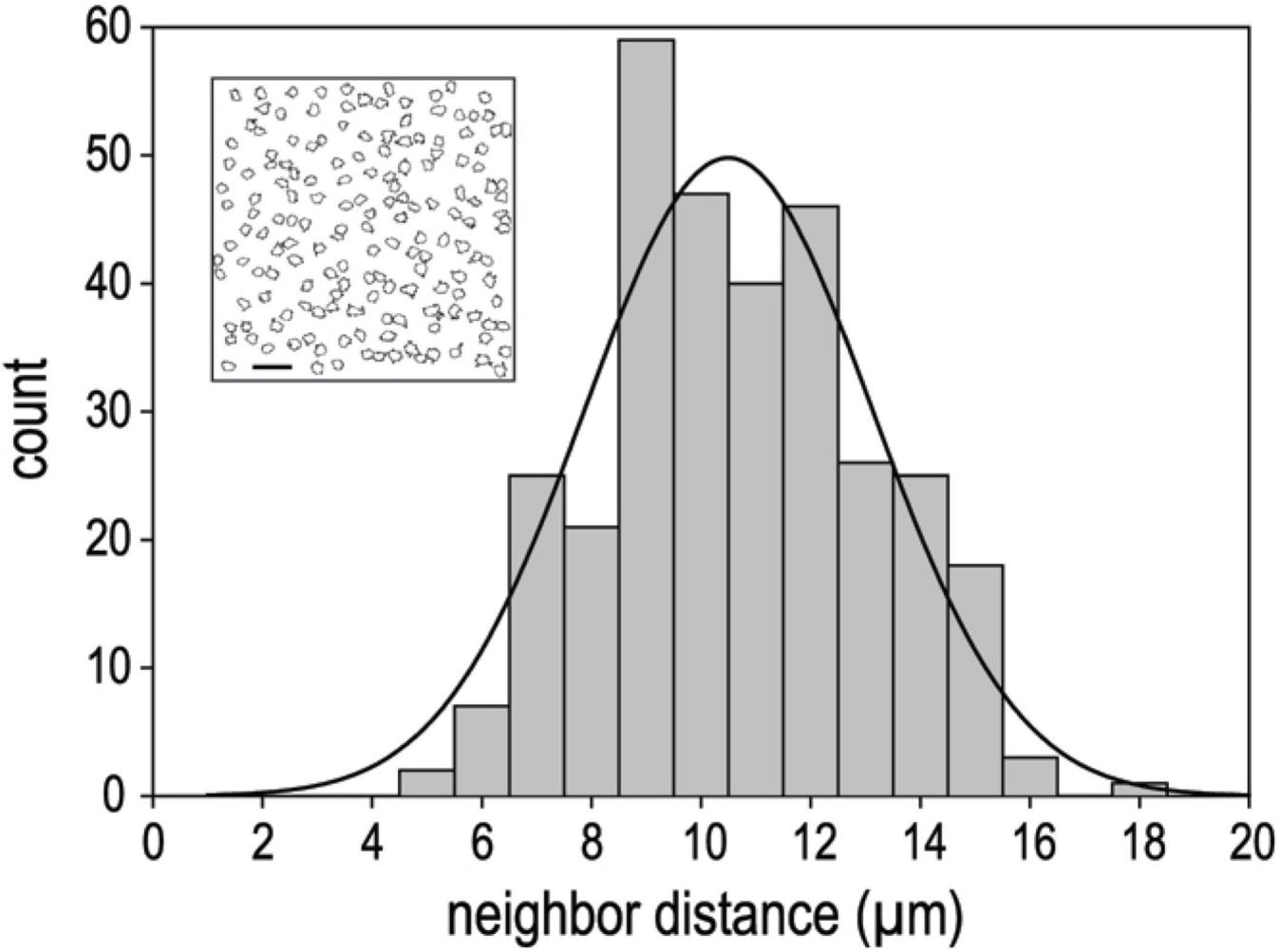

Figure 7.

Nearest neighbor analysis. Histogram of nearest neighbor distances for the DARPP-32 positive cells in Figure 6, panel **C**. The overlaying curve is a best-fit single Gaussian. The corresponding mean inter-soma distance of the Gaussian fit is 10.5 μm (± 0.2 μm, Standard Error). The inset is the result of the Threshold and Particle analysis performed in ImageJ, showing cell outlines selected for nearest neighbor determination. Scale bar is 25 μm.

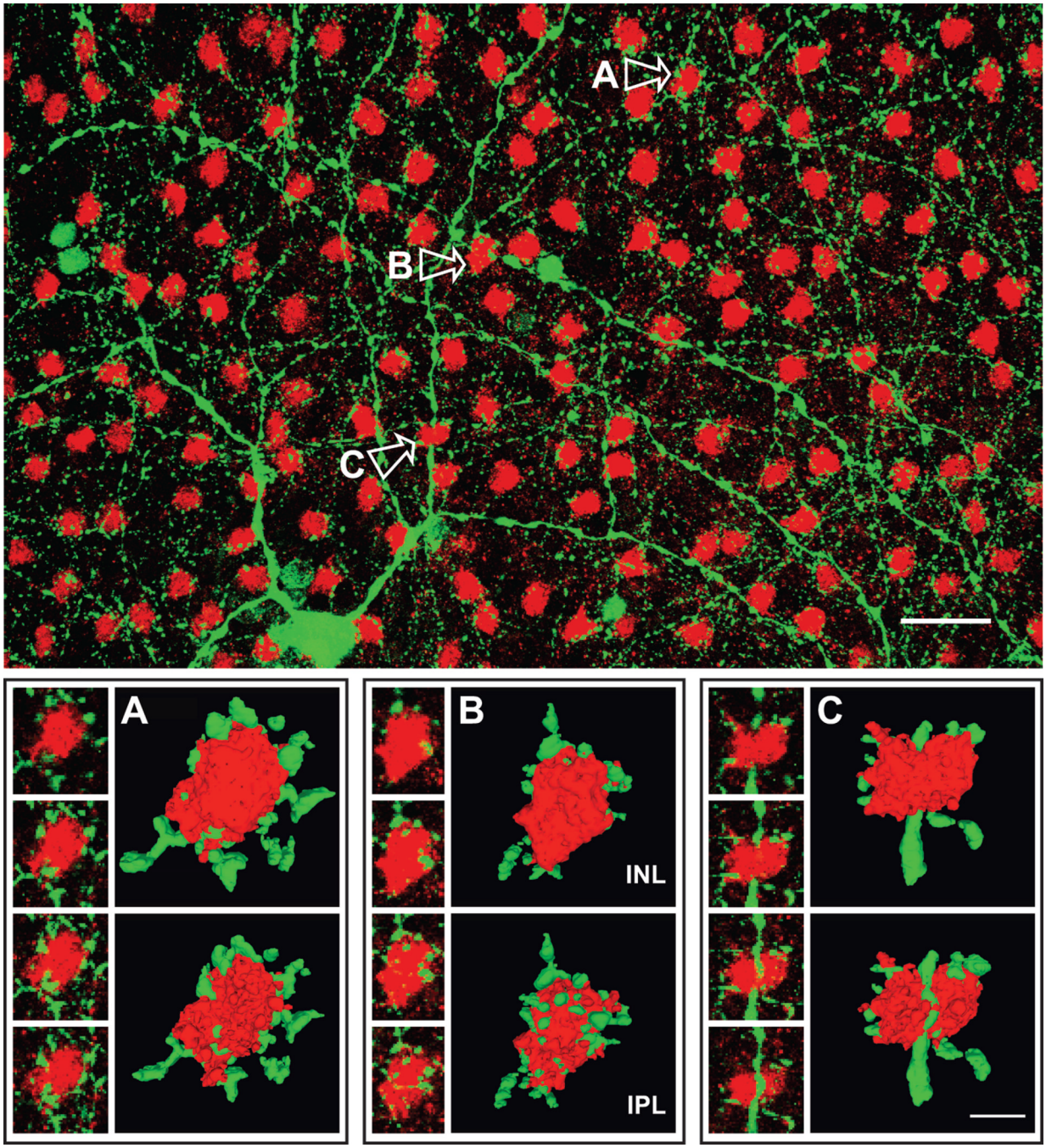

Figure 8.

Colocalization of tyrosine hydroxylase (TH) and DARPP-32 in whole retina. The upper panel is an overlay image of TH-positive cells (green) visualized with anti-TH antibody and Alexa Fluor 488-conjugated anti-mouse IgG and DARPP-32-positive cells (red) stained with anti-DARPP-32 and Alexa Fluor 594. Confocal images were obtained at 0.30 μm z intervals with 2-frame Kalman averaging. This image is a maximum intensity z-projection of 5 consecutive optical sections. The scale bar is 25 μm. The small images in each of the lower panels are high magnification single optical sections of the DARPP cells and associated TH processes labeled **A–C** in the upper panel. These are alternate sections, spaced 0.6 μm apart, and the direction of movement going from the top image down is toward the vitreous. Next

to these are corresponding 3D reconstructions rendered in the image analysis program Volocity. For each cell, we show the face-on view as the cell would look from inside the inner nuclear area (INL) and the view of the opposite side facing the inner plexiform layer (IPL). Each pair of images was constructed by progressing in the same direction through the stack of optical sections; the second view in each pair was then rotated 180° about the y-axis, so that structures in the paired images can be more easily compared. These reconstructions utilized 25 consecutive optical sections of DARPP-32, TH image pairs from which the overlay images shown to the left were drawn. The scale bar in C is 5 μm, and the 3D images in all panels are shown at the same magnification.